Marine Geology 443 (2022) 106665

Contents lists available at ScienceDirect

Marine Geology

journal homepage: www.elsevier.com/locate/margo

Short communication

Discovery of enigmatic toroidal carbonate concretions on the Rio Grande Rise (Southwestern Atlantic Ocean)

Christian Millo [a,*], Matheus H. Vieira do Nascimento e Silva [a], Renata Moura de Mello [b], R. Mark Leckie [c], Mariana Benites [a], Paulo C. Fonseca Giannini [d], Paulo C. Boggiani [d], Dan Bosence [e], Paul A.J. Lusty [f], Bramley J. Murton [g], Luigi Jovane [a]

[a] Instituto Oceanográfico, Universidade de São Paulo, Praça do Oceanográfico 191, CEP 05508-900 São Paulo (SP), Brazil
[b] PETROBRAS Research and Development Center, Av. Horacio de Macedo 950, CEP 21941-915, Rio de Janeiro (RJ), Brazil
[c] Department of Geosciences, University of Massachusetts, 627 N. Pleasant St., Amherst, MA 01003, USA
[d] Instituto de Geociências, Universidade de São Paulo, Rua do Lago, 562, CEP 05508-080, São Paulo (SP), Brazil
[e] Department of Earth Sciences, Royal Holloway University of London, Egham Hill, Egham TW20 0EX, UK
[f] British Geological Survey, Environmental Science Centre, Nottingham NG12 5GG, UK
[g] National Oceanography Centre, Waterfront Campus, Southampton SO14 3ZH, UK

ARTICLE INFO

Editor: Michele Rebesco

Keywords:
Rio Grande Rise
Grainstone
Stable isotopes
Foraminifera
Diagenesis
Remotely operated vehicles

ABSTRACT

We present enigmatic toroidal carbonate concretions retrieved from 700 m water depth from two sites in the upper plateau of the Rio Grande Rise. The concretions have a diameter of ~15 cm and a central hole of ~5 cm, and were observed on top of loose bioclastic sand over an area of ~30 m^2 at 0.5–1.5 m from one another. They consist of brown, porous, bioclastic grainstone, lacking internal structures. Grains consist of sand (< 3% coarse, 30% medium, 35% fine, 25% very fine), composed mainly by planktonic foraminiferal tests, and < 10% lime mud. The observed foraminiferal species indicate initial deposition of the sand in an open ocean setting. Biostratigraphy suggests an age no older than Pleistocene. Petrographic thin sections and SEM reveal that the fossiliferous grainstone contains intraclastic micritic cement and isopachous rim cement made of bladed magnesian calcite. $\delta^{18}O$ values range from +1.5 to +3.3‰ (V-PDB) and increase with the degree of cementation, while $\delta^{13}C$ ranges from +0.5 to +2.3‰ irrespective of cementation. The cementation of the grainstones is likely to have taken place in the marine phreatic environment. Carbonate precipitation induced by methane oxidation or (subaerial) meteoric diagenesis are ruled out based on both cement fabric and isotopic composition. Plausible causes for the toroidal shape of these structures could be: 1) sediment excavation by organisms, or 2) cementation within biofilms around burrows, followed by selective seafloor erosion. However, unveiling the actual formation mechanisms warrants further investigation.

1. Introduction

In January–February 2018 a scientific cruise took place on board the Brazilian R/V *Alpha Crucis* to conduct multidisciplinary oceanographic studies in the western Rio Grande Rise, with focus on marine mineral deposits (Jovane et al., 2019). During scientific dredging, peculiar toroidal concretions, not previously reported in the literature, were recovered (Fig. 1a–d). The concretions consist of brown, cemented bioclastic carbonate sands, 12–15 cm in diameter with a central hole of 4–6 cm. Sectioned samples show neither stratification nor preferential grain orientation. In some case, millimetric to centimetric cavities are visible (Fig. 1d and supplementary material Fig. S1).

In October–November 2018 the RRS *Discovery* sailed to the same area (Fig. 2a–c), equipped with the Remotely Operated Vehicle (ROV) HyBIS. During a ROV dive at 700 m water depth (mwd), the HyBIS submarine camera revealed the presence of these toroidal concretions (at 0.5–1.5 m from one another), on top of loose bioclastic sand (enriched in planktic foraminifera and pteropods) on a ~ 30 m^2-wide gentle slope bordering tabular ferromanganese crusts (Fig. 2d and S2a). No macroorganisms were observed nearby the concretions or encrusting them (Fig. S2b). Similar rounded concretions, lacking the central hole, were also observed (Fig. S2a). One of these (Fig. 1e–f) was collected using the ROV

* Corresponding author.
E-mail address: millo@usp.br (C. Millo).

https://doi.org/10.1016/j.margeo.2021.106665
Received 21 May 2021; Received in revised form 4 October 2021; Accepted 7 October 2021
Available online 13 October 2021

grab arm. The aim of this study is to present a first description of these intriguing concretions, based on thin sections, Scanning Electron Microscope (SEM) micrographs, and micropaleontological and stable isotope data. A preliminary discussion of their possible formation mechanisms is presented.

2. Regional setting

The Rio Grande Rise (RGR) (32°S, 35°W) is a ~ 150,000 m^2 wide oceanic rise located ~1200 km to the east of Brazil and 2000 km to the west of the Mid-Atlantic Ridge (Jovane et al., 2019; Montserrat et al., 2019) (Fig. 2a). It rises from the surrounding abyssal plain (3800 m) to form a plateau of ~700 m, cut in NW–SE direction by a 1300 m deep, 24 km wide channel with steep, 600 to 1000 m high walls (Fig. 2b–c). This channel is part of the Cruzeiro do Sul crustal lineament (Galvão and de Castro, 2017) extending from the oceanic crust towards the continent (Mohriak et al., 2010). Camboa and Rabinowitz (1984) divided the RGR into a western and an eastern portion, with different geological histories. Early studies proposed that the RGR formed 85 million years ago (Ma) from a spreading axis close to the Tristan da Cunha hotspot, from which it was isolated at 70 Ma, leading to separation from its conjugate margin of the Walvis Ridge (O'Connor and Duncan, 1990; Rohde et al., 2013). Subaerial volcanism created the western RGR at 80–85 Ma, followed by subsidence, uplift and more recent subaerial volcanism during the Eocene (40–55 Ma) (Camboa and Rabinowitz, 1984). Subsequently, seafloor spreading and crustal subsidence shifted the RGR to its present position.

3. Materials and methods

The toroidal concretions were found in two sites, at similar water depths and located ~35 km apart on opposite sides of the RGR submarine channel (Fig. 2c). The samples collected during the *Alpha Crucis* cruise (Fig. 1a–d) were dredged from the western RGR plateau near the western flank of the Cruzeiro do Sul channel. Dredging locations were 30.854°S, 36.009°W, 687 mwd and 30.868°S, 36.000°W, 701 mwd (full details in Jovane et al., 2019). The sample collected during the *Discovery* cruise (Fig. 1e–f) was retrieved with the HyBIS grab arm from the eastern rim of the channel, at 30.694°S, 35.745°W, 709 mwd. Unlike dredging, collection by ROV ensured retrieval of a complete sample, accurate positioning and video recording of the original sample orientation. This sample was studied by means of thin sections, grain size analysis, optical microscopy, micropaleontology, SEM, and stable isotope analyses.

A 1.5-cm thick slab (Fig. 1f) was obtained using a water-cooled diamond wire saw. The cuttings were collected, gently disaggregated with a ceramic pestle and mortar, dried at 40 °C and sieved according to the 1 phi (ϕ) classes of the Wentworth (1922) - Krumbein (1938) scale

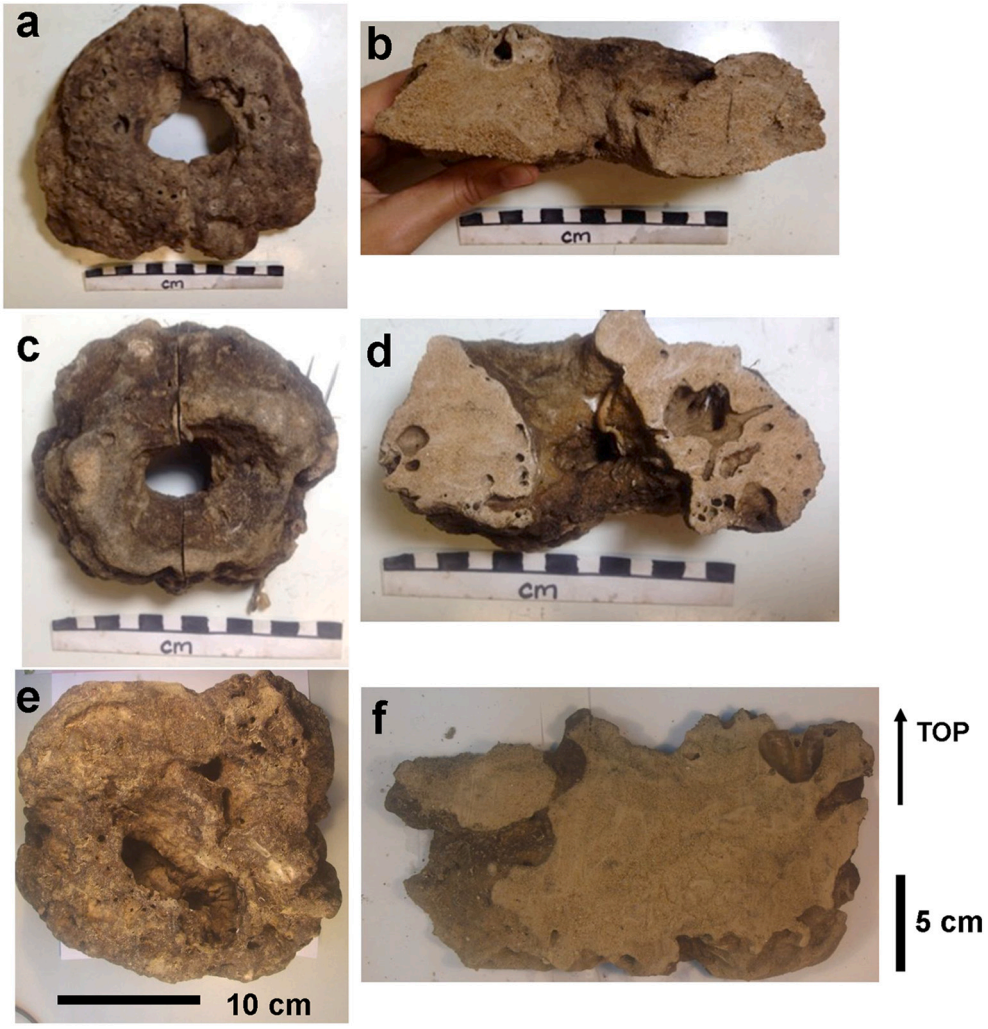

Fig. 1. (a–d) Whole samples and respective cross-sections (b and d) of the toroidal carbonate concretions dredged from the western flank of the Cruzeiro do Sul channel. (e–f) Whole sample and cross-section of the carbonate concretion recovered by the ROV HyBIS on the eastern flank of the Cruzeiro do Sul channel. Scale bars in (a–d) = 12 cm.

between 1.0 mm and 0.062 mm. Each size fraction was weighed and observed under a binocular microscope.

For $\delta^{18}O$ and $\delta^{13}C$ analyses, the sieved samples were subdivided into three categories, according to their apparent degree of cementation under the binocular (Fig. S3).

Category I: Poor cementation. Isolated foraminiferal tests with "sugary" surficial texture indicative of calcite overgrowths;

Category II: Moderate cementation. Bioclast aggregates with tests visible under binocular microscope;

Category III: High cementation. Grey cement aggregates with bioclasts no longer visible.

The rationale was to investigate if highly cemented samples presented an isotopic shift relative to medium and poorly cemented samples, in order reconstruct the diagenetic environment based on the cement isotopic signature (the standard method for stable isotope analysis is outlined in the supplementary material). Part of the 1.5-cm thick slab was ground smooth following standard procedure to produce 30 and 100 μm thin sections for petrographic and SEM observations, respectively.

4. Results

Visual observation of the broken-off hand specimens (Fig. 1) does not reveal the occurrence of fractures or sedimentary structures. Numerous millimetric to centrimetric burrows are visible on the surface, devoid of organisms (Fig. S2b). Grain size fraction percentages are as follows: coarse sand 2.4%, medium sand 30.3%, fine sand 35.0%, very fine sand 24.4%, silt and clay 7.9%. Inspection under binocular microscope revealed the absence of terrigenous sediment. The sample consists entirely of bioclasts with strong dominance of the planktonic foraminiferal species *Globorotalia inflata, Globorotalia truncatulinoides, Globorotalia menardii,* and *Orbulina universa,* followed by *Globigerinoides conglobatus, Globorotalia hirsuta, Globigerinoides sacculifer, Sphaeroidinella dehiscens,* and *Globigerina bulloides*. Benthic foraminifera (e.g., *Uvigerina* spp. and *Cibicidoides wuellerstorfi*) are less abundant, followed by echinoderm and bryozoan fragments, and pteropods. The foraminiferal tests and the other bioclasts are relatively well preserved.

Observation of petrographic thin sections reveals the absence of both intergranular carbonate mud and components larger than 2 mm (Fig. 3a–b). The texture can therefore be classified as fossiliferous grainstone (Dunham, 1962; Embry and Klovan, 1971; Lokier and Al Junaibi, 2016). Cement occurs either within foraminifera chambers or as thin (<5 μm) fringes around bioclasts (Fig. 3a–c and Fig. S4) whereas the remaining interparticle space is unfilled (black space in Fig. 3b and violet areas in Fig. S5). SEM micrographs show cement overgrowth masking test ultrastructures and suturing contacts between bioclasts (Fig. 3d and Fig. S6). The fabric of intra-chamber cement consists of ~2 μm thick, Mg-calcite isopachous bladed spar, with triangular upper terminations (Fig. 3e and Fig. S6–7). Magnesium concentration is highest around external chamber walls (Fig. S5d). These features are similar to Mg-calcite syntaxial cements that are well known diagenetic features in carbonate sediments and limestones (e.g., Bathurst, 1971; Tucker and Wright, 1990).

Energy Dispersive X-Rays Spectroscopy (EDS) elemental mapping of

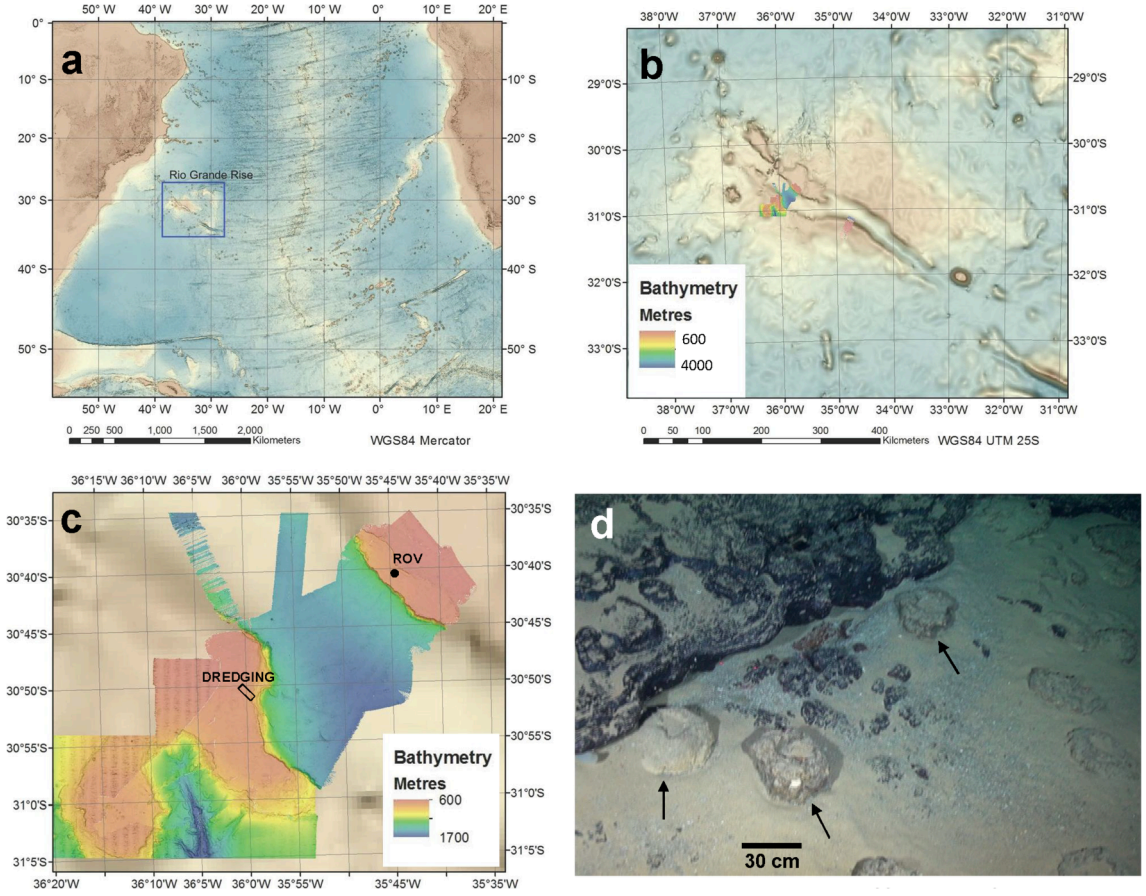

Fig. 2. (a) Location of the RGR in the southwestern Atlantic Ocean. (b) Bathymetric map of the western RGR (area corresponding to the square in (a). The NW-SE oriented central depression is the Cruzeiro do Sul channel. (c) Bathymetric map of the area covered by the RRS *Discovery* cruise in October 2018. Rectangle indicates where the toroidal concretions were dredged during the R/V *Alpha Crucis* cruise in January 2018 (see Fig. 1 (a–d)). The dot indicates the location of the concretion retrieved by ROV in October 2018 (see Fig. 1 (e–f)). (d) ROV photo of toroidal concretions (arrows) outcropping from loose sediment located on a gentle slope bordering tabular ferromanganese crusts (left). Rounded concretions, lacking a characteristic toroidal shape, are also visible (right).

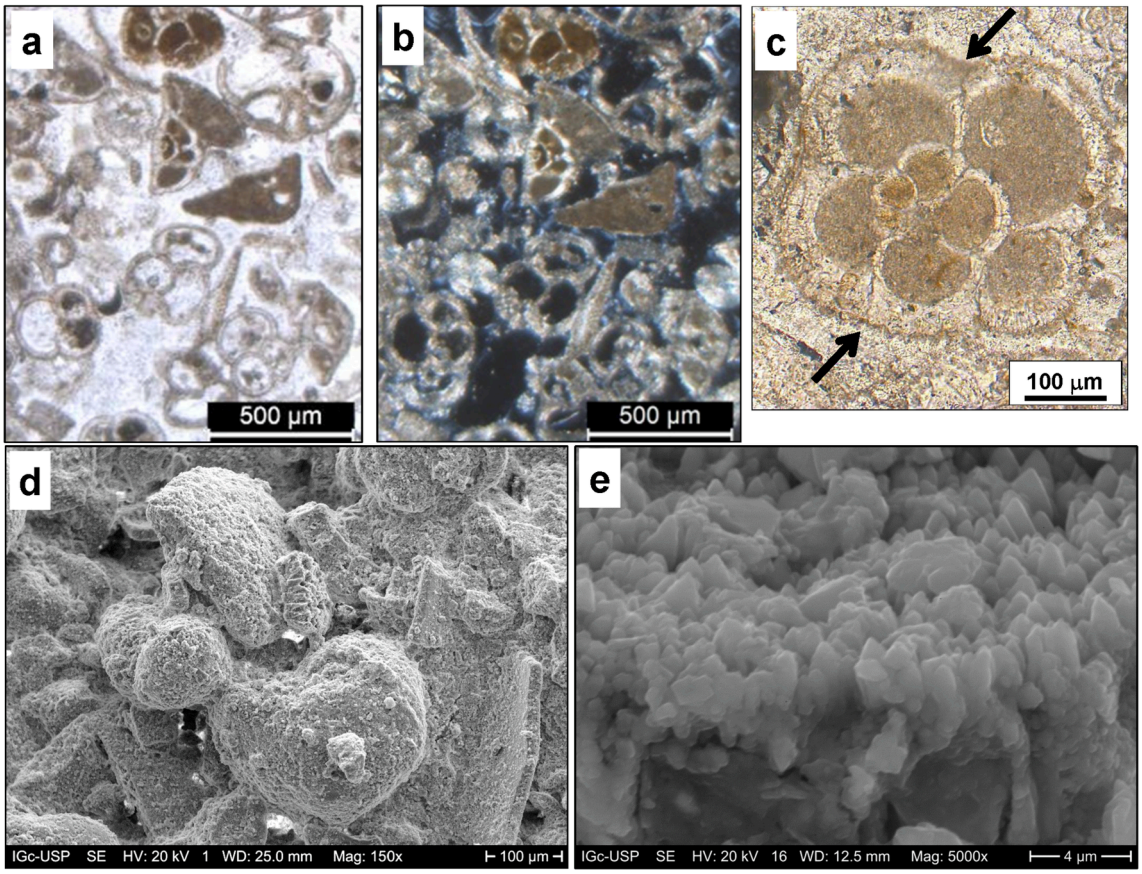

Fig. 3. (a–c) Thin sections of the concretion retrieved by ROV (see Fig. 1 (e–f)). (a) Panoramic thin section showing the fossiliferous grainstone dominated by planktonic foraminiferal tests. Fragments of echinoderms are also present. (Plane polarized light). (b) Crossed-nicols view of (a) showing rim cement suturing the contacts between bioclasts. Black (totally extinct) areas are unfilled intergranular spaces. (c) Carbonate micrite cement (brown) filling foraminiferal chambers. Arrows indicate a thin isopachous rim of carbonate around the foraminiferal test, which can be interpreted either as rim cement or as a microbially-induced micrite envelope (Plane polarized light). (d) SEM micrograph of a fresh broken-off surface showing cement overgrowth suturing the contacts between bioclasts. (e) Isopachous bladed spar cement lining the interior of a chamber wall. This cement consists of euhedral crystals of magnesian calcite (see supplementary material Fig. S7) with c-axes growing orthogonally to the chamber wall. (For interpretation of the references to colour in this figure legend, the reader is referred to the web version of this article.)

fresh broken-off surfaces show strong signals of Ca and Mg and low signals for Al, K, Mn, and Fe, with no preferential element distribution in the samples (Fig. S8–10).

The results of stable isotope analyses are as follows (N = number of analyses):

Category I: *Globigerinoides* spp. ($N = 3$) $\delta^{18}O = +1.7$ to $+2.3$‰; $\delta^{13}C = +1.8$ to $+2.3$‰;

G. hirsuta (N = 3) $\delta^{18}O = +1.5$ to $+2.2$‰; $\delta^{13}C = +1.8$ to $+2.1$‰;

Category II ($N = 6$): $\delta^{18}O = +2.1$ to $+3.3$‰; $\delta^{13}C = +0.5$ to $+2.0$‰;

Category III (N = 6): $\delta^{18}O = +2.9$ to $+3.3$‰; $\delta^{13}C = +2.0$ to $+2.2$‰.

$\delta^{18}O$ and $\delta^{13}C$ ranges are similar in isolated tests of *Globigerinoides* spp. and *G. hirsuta*. On average, $\delta^{18}O$ values increase by ~1.0 to 1.5‰ from poorly- to highly cemented samples. $\delta^{13}C$ values are similar in Categories I and III, while Category II shows an internal variability of 1.5‰ (Fig. S11).

5. Discussion and conclusion

The measured grain size distribution results from the fact that the sample is mainly composed by planktonic foraminiferal tests, the sizes of which fall in the medium to very fine sand granulometric fractions. The mud-sized fraction consists essentially of test fragments plus cement disaggregated during sample preparation and sieving, whereas the coarse sand consists mainly of highly-cemented aggregates (cementation Category III).

The observed planktonic foraminiferal species are typical of the mixed-layer, thermocline, and/or subthermocline oceanic habitats (Steph et al., 2009; Birch et al., 2013; Sousa et al., 2014), indicating deposition in a subtropical, oceanic setting (Bé, 1977; Vincent and Berger, 1981; Lam and Leckie, 2020). In terms of biostratigraphy, the presence of *G. truncatulinoides* suggests an age no older than Pleistocene (Wade et al., 2011).

The observed cement fabric is reported in the literature as a typical product of marine phreatic diagenesis (Bathurst, 1971; Marshall and Ashton, 1980; Tucker and Wright, 1990; Noé et al., 2006; Christ et al., 2015). In particular, the fabric of the isopachous bladed spar lining the interior chamber walls of foraminifera, made up by euhedral crystals with c-axes growing orthogonally to the walls (Fig. 3e), is similar to that of syndepositional and early diagenetic cements reported both by Noé et al. (2006) from 663 to 790 mwd at the western Rockall Bank and Porcupine Bank (northeastern Atlantic Ocean), and by Tucker et al. (2020) from 806 mwd, from the SW of the island of Montserrat (Caribbean).

Early diagenetic cementation is suggested by the presence of interparticle porosity and isopachous rim cement at the contact points between tests (Fig. 3a–c and Fig. S4). The rim cements are associated with dark, fine-grained rims to the grains similar to micrite envelopes (Fig. 3c). Such envelopes form by alteration of carbonate grains by endolithic microorganisms (Bathurst, 1971). The isopachous calcite cement and the micrite envelopes consistently suggest a marine phreatic

early diagenetic environment. In alternative, the rim cements could be interpreted as carbonate sutures formed by dissolution/reprecipitation.

The measured $\delta^{18}O$ and $\delta^{13}C$ values, further suggest a marine phreatic early diagenetic environment. The range of $\delta^{18}O$ and $\delta^{13}C$ values of our samples are in the range of those presented by Tucker et al. (2020) for carbonate crusts from 180 to 820 mwd, around the island of Montserrat ($\delta^{18}O = +1.06$ to $+2.78‰$; $\delta^{13}C = +1.95$ to $+3.71‰$), the Kick'em Jenny submarine volcano (Caribbean) ($\delta^{18}O = +2.11‰$; $\delta^{13}C = +2.61‰$), and the Kolumbo submarine volcano (Mediterranean Sea) ($\delta^{18}O = +2.80$ to $+3.04‰$; $\delta^{13}C = +1.89$ to $+3.17‰$). A similar isotopic range was also reported for mid-Pleistocene hardgrounds from the Rockall and Porcupine Banks ($\delta^{18}O = +2.5$ to $+3.6‰$; $\delta^{13}C = +0.5$ to $+1.2‰$) (Noé et al., 2006).

The observed 1.0 to 1.5‰ $\delta^{18}O$ increase from poorly- to highly cemented samples (Fig. S11) suggests cement formation at lower temperature relative to primary foraminiferal calcite (~4 to 6 °C decrease assuming isotopic equilibrium with seawater). The positive correlation between $\delta^{18}O$ and degree of cementation is a typical feature observed in lithified limestones of different locations and ages (Allouc, 1990; Aghib et al., 1991; James and Bone, 1992; Christ et al., 2015) and reinforces the interpretation that the lithology that forms these concretions was deposited and cemented in a marine phreatic environment.

The possible explanations for the toroidal shape of these concretions remain speculative. Contrast comparison with similar features does not offer a satisfactory analogue. Initially, the characteristic shape of these structures suggested that the central cavities could have been originally occupied by root systems and/or stumps, in analogy to the fossil forest of the Jurassic Purbeck Formation (Dorset, England) (Francis, 1984). This initial hypothesis was discarded both because the micropaleontological observations indicate an open-ocean sedimentary environment and because the marine oxygen isotope signature does not indicate subaerial exposure or meteoric diagenesis. An alternative initial hypothesis was that the concretions had a stromatolitic origin. Although their round shape and arrangement on the seafloor may recall those of a columnar stromatolite field, the interior of the toroidal concretions lack a characteristic clotted or laminated internal texture and shows no SEM evidence of microbial features.

The presence of the characteristic ~5 cm central hole and of smaller internal cavities (Fig. 1d and Fig. S1) might attest to fluid or gas migration through the concretions. However, the $\delta^{18}O$ values indicate cementation at a relatively low temperature, excluding the potential role of geothermal fluids, whereas the positive $\delta^{13}C$ values exclude cement precipitation linked to methane seepage and oxidation, with would result in negative $\delta^{13}C$ values (Dickens et al., 1995; Kennett et al., 2000; Peckmann et al., 2002; Hill et al., 2004; Millo et al., 2005; Gabitov et al., 2019; Buckman et al., 2020).

Another hypothesis could be excavations by crustaceans, which can stabilize their burrows with mucus and leave a variety of trace fossils (Swen et al., 2001; Taviani et al., 2015 and references therein; Sparacio et al., 2020). This hypothesis is highly speculative, both because the concretions showed no fossil evidence of crustaceans and because no macroorganisms were observed nearby the concretions (ROV images in Fig. 2d and Fig. S2).

Regardless the burrowing mechanism, the walls to the central cavity could have induced cementation of the surrounding bioclastic sand, preventing subsequent erosion. Differential cementation around burrows is reported from the geological record, and in particular in deep-water carbonate sediments (e.g., Eren and Tasli, 2002; James and Jones, 2016; Yeomans, 2019). Cementation could have occurred due to the presence of oxygenated water in the burrows, causing the oxidation of organic matter associated with bioclasts and leading to a pH decrease, partial dissolution of tests and reprecipitation of early diagenetic rim cements around the burrows (Molenaar and Zijlstra, 1997). In alternative, weakly-hardened sediment around burrows could be stabilized by biofilms. This remains a viable hypothesis for future investigation, because the detection of biofilms on the surface of our samples was beyond the original scope of the study.

The formation mechanism of these structures remains enigmatic, but their occurrence in two locations on opposite sides of the RGR submarine channel suggests that they might have a wider significance in terms of hardground formation in the study area. The spatial and age distribution of hardgrounds in the RGR has not been thoroughly studied yet, and will be investigated in a future project.

Author contributions

C.M.: Investigation, Data curation, Writing - Original Draft. M.H.V.N. S. and M.B.: Sample preparation. R.M.M. and R.M.L.: Micropaleontological investigation. P.C.B.: Laboratory coordination. D.B. and P.C.F.G.: Carbonate petrography. P.A.J.L. and B.J.M.: RRS *Discovery* Chief Scientists, Funding acquisition (UK). L.J.: R/V *Alpha Crucis* Chief Scientist, Funding acquisition (Brazil). All authors have contributed to the scientific discussion of the data presented.

Data availability

The stable isotope data presented in this study are available at: https://doi.org/10.17632/45hw8sy2wx.1

Declaration of Competing Interest

The authors declare that they have no known competing financial interests or personal relationships that could have appeared to influence the work reported in this paper.

Acknowledgements

This work was supported by the Natural Environment Research Council (NERC, grant number NE/MO11151/1) and by the Fundação de Amparo a Pesquisa do Estado de São Paulo (FAPESP, grant number 2014/50820-7).

We thank the ROV HyBIS engineers, the captains, the officers and crews of the R/V *Alpha Crucis* and RRS *Discovery*, Dr. Isaac J. Sayeg for SEM images, Alyne Barros and Luciana Nogueira for technical assistance. We are grateful to the Editor, Dr. M. Rebesco, and to Dr. A. Immenhauser and two anonymous reviewers for their constructive and insightful comments, which greatly improved the manuscript.

Appendix A. Supplementary data

Supplementary data to this article can be found online at https://doi.org/10.1016/j.margeo.2021.106665.

References

Aghib, F.S., Bernoulli, D., Weissert, H., 1991. Hardground formation in the Bannock Basin, Eastern Mediterranean. Mar. Geol. 100, 103–113. https://doi.org/10.1016/0025-3227(91)90227-U.

Allouc, J., 1990. Quaternary crusts on slopes of the Mediterranean Sea: a tentative explanation for their genesis. Mar. Geol. 94, 205–238. https://doi.org/10.1016/0025-3227(90)90070-Z.

Bathurst, R.G.C., 1971. Carbonate Sediments and their Diagenesis. Elsevier, p. 620.

Bé, A.W.H., 1977. An ecological, zoogeographic and taxonomic review of recent planktonic foraminifera. In: Ramsay, A.T.S. (Ed.), Oceanic Micropaleontology. Academic Press, London.

Birch, H., Coxall, H.K., Pearson, P.N., Kroon, D., O'Regan, M., 2013. Planktonic foraminifera stable isotopes and water column structure: Disentangling ecological signals. Mar. Micropaleontol. 101, 127–145. https://doi.org/10.1016/j.marmicro.2013.02.002.

Buckman, J., Donnelly, T., Jiang, Z., Lewis, H., Ruffell, A., 2020. Methane derived authigenic carbonate (MDAC) aragonite cemented quaternary hardground from a methane cold seep, Rathlin Basin, Northern Ireland: $\delta^{13}C$ and $\delta^{18}O$ isotopes, environment, porosity and permeability. Geosciences. 10, 255–273 doi.10.10.3390/geosciences10070255.

Camboa, L.A.P., Rabinowitz, P.D., 1984. The evolution of the Rio Grande Rise in the Southwest Atlantic Ocean. Mar. Geol. 58, 35–58. https://doi.org/10.1016/0025-3227(84)90115-4.

Christ, N., Immenhauser, A., Wood, R.A., Darwich, K., Niedermayr, A., 2015. Petrography and environmental controls on the formation of Phanerozoic marine carbonate hardgrounds. Earth Sci. Rev. 151, 176–226. https://doi.org/10.1016/j.earscirev.2015.10.002.

Dickens, G.R., O'Neil, J.R., Rea, D.K., Owen, R.M., 1995. Dissociation of oceanic methane hydrate as a cause of the carbon isotope excursion at the end of the Paleocene. Paleoceanography 10, 965–971. https://doi.org/10.1029/95PA02087.

Dunham, R.J., 1962. Classification of carbonate rocks according to depositional texture. In: Ham, W.E. (Ed.), Classification of Carbonate Rocks, 1. American Association of Petroleum Geologists Memoire, pp. 108–121.

Embry, A.F., Klovan, J.E., 1971. A Late Devonian reef tract on northeastern Banks Island, N.W.T.1. Bull. Can. Petrol. Geol. 19, 730–781. https://doi.org/10.35767/gscpgbull.19.4.730.

Eren, M., Tasli, K., 2002. Kilop cretaceous Hardground (Kale, Gümüshane, NE Turkey): description and origin. J. Asian Earth Sci. 20, 433–448. https://doi.org/10.1016/S1367-9120(01)00027-X.

Francis, J.E., 1984. The seasonal environment of the Purbeck (Upper Jurassic) fossil forests. Palaeogeogr. Palaeoclimatol. Palaeoecol. 48, 285–307. https://doi.org/10.1016/0031-0182(84)90049-X.

Gabitov, R., Borrelli, C., Buettner, J., Kirkland, B., Skarke, A., Trail, D., Garner, B., Testa, M., Wahidi, M., Hoff, C., Khasanov, S., Panieri, G., Thirumalai, R., Thomas, J., Weremeichik, J., Zverkova, I., 2019. Characterization of carbonate crust from a recently discovered Methane Seep on the North Atlantic Continental Margin of the USA. Minerals 9. https://doi.org/10.3390/min9030138.

Galvão, I.L.G., de Castro, D.L., 2017. Contribution of global potential field data to the tectonic reconstruction of the Rio Grande Rise in the South Atlantic. Mar. Pet. Geol. 86, 932–949. https://doi.org/10.1016/j.marpetgeo.2017.06.048.

Hill, T.M., Kennett, J.P., Spero, H.J., 2004. High-resolution records of methane hydrate dissociation: ODP Site 893, Santa Barbara Basin. Earth Planet. Sci. Lett. 223, 127–140. https://doi.org/10.1016/j.epsl.2004.04.003.

James, N.P., Bone, Y., 1992. Synsedimentary cemented calcarenite layers in Oligo-Miocene cool- water shelf limestones, Eucla Platform, southern Australia. J. Sediment. Petrol. 62, 860–872. https://doi.org/10.1306/D42679FB-2B26-11D7-8648000102C1865D.

James, N.P., Jones, B., 2016. Origin of Carbonate Sedimentary Rocks. Wiley, p. 446.

Jovane, L., Hein, J.R., Yeo, I.A., Benites, M., Bergo, N.M., Corrêa, P.V.F., Couto, D.M., Guimarães, A.D., Howarth, S.A., Miguel, H.R., Mizell, K.L., Moura, D.S., Vicentini Neto, F.L., Pompeu, M., Rodrigues, I.M.M., Santana, F.R., Serrao, P.F., Silva, T.E., Tura, P.M., Viscarra, C.L., Chuqui, M.G., Pellizari, V.H., Signori, C.N., Da Silveira, I. C.A., Sumida, P.Y.G., Murton, B.J., Brandini, F.P., 2019. Multidisciplinary Scientific Cruise to the Rio Grande Rise. Front. Mar. Sci. 6 https://doi.org/10.3389/fmars.2019.00252.

Kennett, J.P., Cannariato, K.G., Hendy, I.L., Behl, R.J., 2000. Carbon isotopic evidence for methane hydrate instability during Quaternary interstadials. Science 288, 128–133. https://doi.org/10.1126/science.288.5463.128.

Krumbein, W.C., 1938. Size frequency distributions of sediments and the normal phi curve. J. Sediment. Res. 8, 84–90. https://doi.org/10.1306/D4269008-2B26-11D7-8648000102C1865D.

Lam, A.R., Leckie, R.M., 2020. Late Neogene and Quaternary diversity and taxonomy of subtropical to temperate planktic foraminifera across the Kuroshio Current Extension, northwest Pacific Ocean. Micropaleontology 66, 177–268. https://doi.org/10.47894/mpal.66.3.01.

Lokier, S.W., Al Junaibi, M., 2016. The petrographic description of carbonate facies: are we all speaking the same language? Sedimentology 63, 1843–1885. https://doi.org/10.1111/sed.12293.

Marshall, J.D., Ashton, M., 1980. Isotopic and trace element evidence for submarine lithification of hardgrounds in the Jurassic of eastern England. Sedimentology 27, 271–289. https://doi.org/10.1111/j.1365-3091.1980.tb01178.x.

Millo, C., Sarnthein, M., Erlenkeuser, H., Grootes, P.M., Andersen, N., 2005. Methane-induced early diagenesis of foraminiferal tests in the southwestern Greenland Sea. Mar. Micropaleontol. 58, 1–12. https://doi.org/10.1016/j.marmicro.2005.07.003.

Mohriak, W.U., Nóbrega, M., Odegard, M.E., Gomes, B.S., Dickson, W.G., 2010. Geological and geophysical interpretation of the Rio Grande Rise, south-eastern Brazilian margin: Extensional tectonics and rifting of continental and oceanic crusts. Pet. Geosci. 16, 231–245. https://doi.org/10.1144/1354-079309-910.

Molenaar, N., Zijlstra, J.J.P., 1997. Differential early diagenetic low-Mg calcite cementation and rhythmic hardground development in Campanian-Maastrichtian chalk. Sediment. Geol. 109, 261–281. https://doi.org/10.1016/S0037-0738(96)00064-4.

Montserrat, F., Guilhon, M., Corrêa, P.V.F., Bergo, N.M., Signori, C.N., Tura, P.M., Santos Maly, M.D.L., Moura, D., Jovane, L., Pellizari, V., Sumida, P.Y.G., Brandini, F.P., Turra, A., 2019. Deep-sea mining on the Rio Grande Rise (Southwestern Atlantic): a review on environmental baseline, ecosystem services and potential impacts. Deep-Sea Res. I Oceanogr. Res. Pap. 145, 31–58. https://doi.org/10.1016/j.dsr.2018.12.007.

Noé, S., Titschack, J., Freiwald, A., Dullo, W.-C., 2006. From sediment to rock: diagenetic processes of hardground formation in deep-water carbonate mounds of the NE Atlantic. Facies 52, 183–208. https://doi.org/10.1007/s10347-005-0037-x.

O'Connor, J.M., Duncan, R.A., 1990. Evolution of the Walvis Ridge-Rio Grande Rise Hot Spot System: implications for African and South American Plate motions over plumes. J. Geophys. Res. Solid Earth 95, 17475–17502. https://doi.org/10.1029/JB095iB11p17475.

Peckmann, J., Goedert, J.L., Thiel, V., Michaelis, W., Reitner, J., 2002. A comprehensive approach to the study of methane-seep deposits from the Lincoln Creek Formation, western Washington State, USA. Sedimentology 49, 855–873. https://doi.org/10.1046/j.1365-3091.2002.00474.x.

Rohde, J.K., van den Bogaard, P., Hoernle, K., Hauff, F., Werner, R., 2013. Evidence for an age progression along the Tristan-Gough volcanic track from new 40Ar/39Ar ages on phenocryst phases. Tectonophysics 604, 60–71. https://doi.org/10.1016/j.tecto.2012.08.026.

Sousa, S.H.M., de Godoi, S.S., Amaral, P.G.C., Vicente, T.M., Martins, M.V.A., Sorano, M. R.G.S., Gaeta, S.A., Passos, R.F., Mahiques, M.M., 2014. Distribution of living planktonic foraminifera in relation to oceanic processes on the southeastern continental Brazilian margin (23°S-25°S and 40°W-44°W). Cont. Shelf Res. 89, 76–87. https://doi.org/10.1016/j.csr.2013.11.027.

Sparacio, C.A., Buynevich, I.V., Curran, H.A., Kopczynski, K., 2020. Morphometry of blue land crab (*Cardisoma guanhumi*) burrows: ichnological context and paleoenvironmental implications. Palaios 35, 461–469. https://doi.org/10.2110/palo.2020.034.

Steph, S., Regenberg, M., Tiedemann, R., Mulitza, S., Nürnberg, D., 2009. Stable isotopes of planktonic foraminifera fromtropical Atlantic/Caribbean core-tops: implications for reconstructing upper ocean stratification. Mar. Micropaleontol. 71, 1–19. https://doi.org/10.1016/j.marmicro.2008.12.004.

Swen, K., Fraaije, R.H.B., van der Zwaan, G.J., 2001. Polymorphy and extinction of the late cretaceous burrowing shrimp Protocallianassa faujasi and first record of the genera Corallianassa and Calliax (Crustacea, Decapoda, Thalassinoidea) from the cretaceous. Contrib. Zool. 70, 85–98. https://doi.org/10.1163/18759866-07002003.

Taviani, M., Franchi, F., Angeletti, L., Correggiari, A., López-Correa, M., Maselli, V., Mazzoli, C., Peckmann, J., 2015. Biodetrital carbonates on the Adriatic continental shelf imprinted by oxidation of seeping hydrocarbons. Mar. Pet. Geol. 66, 511–531. https://doi.org/10.1016/j.marpetgeo.2015.03.015.

Tucker, M., Wright, V.P., 1990. Carbonate Sedimentology. Blackwells, p. 482.

Tucker, M.E., Carey, S.N., Sparks, R.S.J., Stinton, A., Leng, M., Robinson, L., Li, T., Lewis, J., Cotton, L., 2020. Carbonate crusts around volcanic islands: Composition, origin and their significance in slope stability. Mar. Geol. 429, 106320. https://doi.org/10.1016/j.margeo.2020.106320.

Vincent, E., Berger, W.H., 1981. Planktonic foraminifera and their use in paleoceanography. In: Emiliani, C. (Ed.), The Oceanic Lithosphere: The Sea, vol. VII. Wiley & Sons, New York, pp. 1025–1119.

Wade, B.S., Pearson, P.N., Berggren, W.A., Pälike, H., 2011. Review and revision of Cenozoic tropical planktonic foraminiferal biostratigraphy and calibration to the geomagnetic polarity and astronomical time scale. Earth Sci. Rev. 104, 111–142. https://doi.org/10.1016/j.earscirev.2010.09.003.

Wentworth, C.K., 1922. A scale of grade and class terms for clastic sediments. J. Geol. 30, 377–392. https://doi.org/10.1086/622910.

Yeomans, R., 2019. Paramoudra: observations on large flint structures from the Chalk (Upper cretaceous) and flint formation. Proc. Yorks. Geol. Soc. 62, 210–216. https://doi.org/10.1144/pygs2017-005.